GEOIDE STRATEGIC INVESTMENT PROJECT

River Ice Monitoring with Synthetic Aperture Radar (SAR)

Final report No R-810-f *April 2005*

GEOIDE STRATEGIC INVESTMENT PROJECT

River Ice Monitoring with Synthetic Aperture Radar (SAR)

Final Report

Submitted to BCHydro

Project Leader:

Monique Bernier, INRS-ETE

Deputy Leader:

Frank Weber, BCHydro

Report No R-810-f

April 15, 2005

ISBN : 978-2-89146-788-9

Project Leader:

Monique Bernier, INRS-ETE

Deputy Leader:

Frank Weber, BCHydro

Research Team:

Yves Gauthier, INRS-ETE

Stéphane Savary, INRS-ETE

Lisa-Marie Pâquet, INRS-ETE

Martin Jasek, BCHydro

Imen Gherboudj, INRS-ETE

Marc Philippin, INRS-ETE

Table of contents

List of figures

List of tables

1 Introduction

In cold climates, the winter regime of rivers and lakes is often a determining factor in the management of water resources. This is particularly true for northern rivers, which freeze up in an upstream direction. For the operation of hydropower generating facilities, knowledge of ice cover formation and break-up, ice types, and ice strength is critical. However, with current techniques it is difficult to obtain the spatial distribution of those parameters for a long river like the Peace River (Alberta). Since 2000, BC HYDRO, in co-operation with RADARSAT International, has been analyzing RADARSAT-1 images of the Peace River in an attempt to derive river ice information from remotely sensed data. Although promising results were obtained, more data needed to be collected and analyzed to validate the relationships between river ice and the SAR signal and to eventually develop operational tools and procedures. This project under the GEOIDE Strategic Investment Initiative was intended to combine the efforts of a private sector industry and the expertise of the scientific community.

The global objective of the project was to provide a reliable ice thickness estimation technique and ice cover type classification from SAR data on the Peace River (Alberta) near the town of Peace River.

The specific objectives were:

1. To validate and strengthen the regression relationship between backscattering coefficients of RADARSAT-1 and ENVISAT-ASAR images and river ice thickness measurements on the Peace River;

2. To classify river ice cover from RADARSAT-1 and ENVISAT-ASAR images using backscatter and texture data;

3. To identify ways to increase the SAR data availability by standardizing the signal from different incident and look angles and by looking at data from other sensors.

The river studied is the Peace River. The unregulated Peace River originated in northeastern British Columbia, west of the Rocky Mountains. In 1972, the construction of the BC Hydro Bennett Dam created Williston Reservoir. The Peace River now originates at the dam and flows for about 1300 km in a northeasterly direction across Alberta before draining into the Slave River. A 60 km long test river reach upstream of the town of Peace River was chosen due to the importance of the reach for the flood protection of the town and ease of access for field work. A 350km long validation river reach stretched from Dunvegan (100km upstream of the town of Peace River) to Carcajou (250km downstream of the town of Peace River).

2 Data collection

2.1 Image acquisitions

RADARSAT and ASAR image acquisitions for the winter of 2003/2004 are summarized in Table 1. Image scheduling is an integral part of river ice monitoring with Fine Beam SAR images. As part of this study, the first image of the test reach was scheduled to be taken shortly after ice cover formation. For that reason BC Hydro recommended to acquire the first RADARSAT-1 image on January 10, since the ice front had just passed the town of Peace River. About 20% of the imaged river reach are ice covered. The next acquisition was ten days later on January 20. On that date the ice front was 40 km upstream of the town and about 80% of the imaged river reach were ice covered. A simultaneous ASAR image was acquired but the image could not be used due to processing problems encountered by the provider. The third RADARSAT-1 acquisition was on January 27, when the entire test reach was ice covered. An ASAR image was acquired during that period on February 1. The area upstream from the test area to Dunvegan was covered on February 13. The final RADARSAT-1 acquisition over the test area was on February 20. Four other RADARSAT-1 images were acquired on the same day to cover the area between TPR and Carcajou. Additional ASAR images were acquired on February 10, 2004 and February 20.

Table 1: Image acquisitions

RADARSAT-1 images (C-band-HH)		ASAR images (C-band-HH-VV)	
Date	**Beam (incidence angles)**	**Date**	**Beam (incidence angles)**
10 January 2004	F4 (43.5°-45.8°)	01 February 2004	IS6 (39.1°-42.8°)
20 January 2004	F1N (36.4°-39.5°)	10 February 2004	IS2 (19.2°-26.7°)
27 January 2004	F2F (39.5°-42.5°)	20 February 2004	IS5 (35.8°-39.4°)
13 February 2004	F2N (38.5°-41.5°)		
20 February 2004 (5x)	F2F (39.5°-42.5°)		

2.2 Georeferencing with corner reflectors

Georeferenced ground control points (GCPs) are used for image georectification. GCPs can include buildings, street corners, striking geologic features, etc. Due to the remoteness of the test area GCPs are scarce and it was decided to build and install three corner reflectors along the river channel. Corner reflectors are made of three right triangular perforated aluminum panels, which are oriented towards the satellite (Figure 1). The sides of the reflectors are 1.2m long. The initial design was provided by C-CORE (St. John's NL) and modified by Neptune Dynamics Ltd. (Richmond, BC). Corner reflectors reflect the incoming radiation from the active satellite system straight back to the satellite, thereby creating a very bright response on the image. The installation sites were chosen to be on or near the river, well distributed on the image, on a dark radar background, and accessible. The exact locations were determined by GPS (+/- 3-5m RMS as given by the GARMIN GPS12).

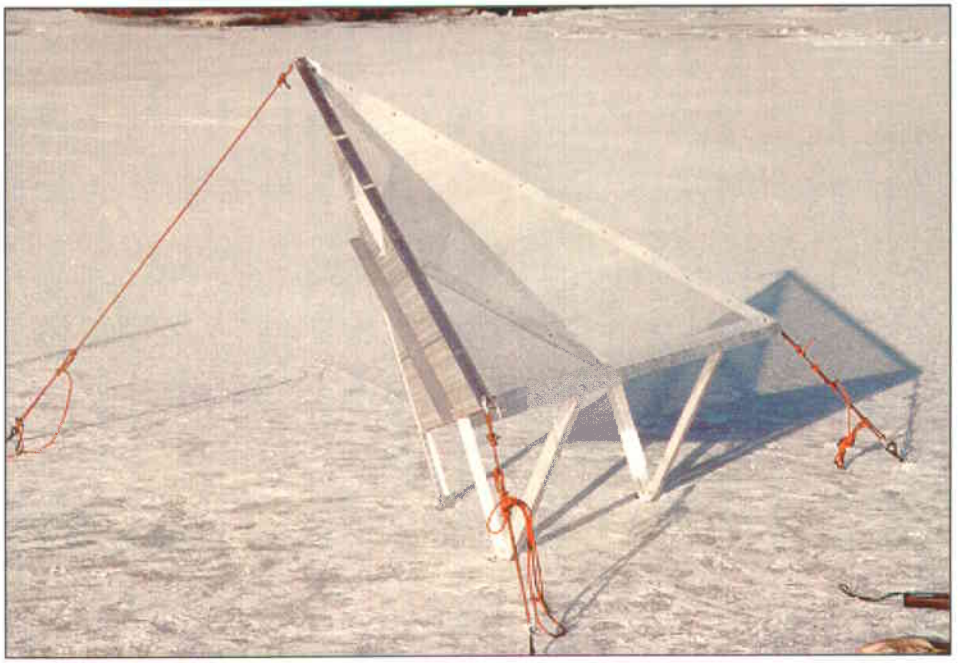

Figure 1: Corner reflector on the Peace River

2.3 Field measurements

During the winter of 2003/2004, BCHydro in collaboration with Alberta Environment and Trillium Engineering (on behalf of Glacier Power) conducted an extensive field program.

Field data were collected on January 18-25, February 18-20, and March 16-18, 2004. The January 18-25 and February 18-20 field trips were scheduled to coincide with image acquisitions. Personnel from INRS-ETE also participated in the February field trip.

Four cross sections were surveyed on each visit. Cross section data consisted typically of 15 samples of snow depth, thermal thickness, total thickness, water level, and 'sail height'. Thermal ice forms between frazil ice pans due to radiative cooling of water. Total ice thickness includes the thickness of thermal ice, which forms on the water surface, the thickness of juxtaposed or consolidated pans, which project down into the water, and frazil slush, which may accumulate below. 'Sail height' is a measure of the surface roughness of the ice cover. It is measured from the thermal ice surface up to the average top of larger protruding pieces of ice by visually lining them up with the horizon. Another measure of the surface roughness of the ice cover is 'chain roughness'. 'Chain roughness' was measured by laying down a chain of known length over the ice and measuring its horizontal length. The shorter the measured length is, the rougher the ice.

Ice front observations during the winter were obtained by Alberta Environment and BC Hydro ice observation flights. BC Hydro, Alberta Environment and Trillium Engineering supplemented these with ground observations. On February 20, 2004 an aerial survey was conducted over the extended area and photos were taken.

2.4 River ice conditions during the monitoring period

Figure 2 summarizes the progression of the ice front as well as the field data collection during the winter 2003-2004. The ice front passed the downstream limit of the extended monitoring area at Carcajou on December 23, 2003. Seventeen days later, on January 9, 2004, the ice front passed the town of Peace River. From January 12-14 the ice front stalled at the confluence of the Peace and Smoky Rivers before reaching the upstream limit of the extended monitoring area at the Dunvegan bridge on January 28, 2004. The cross section surveys in the town of Peace River were conducted approximately 13, 41, and 68 days after freeze-up. On January 30, 2004, a major consolidation occurred upstream of Dunvegan and approximately 80 km of ice collapsed to approximately 55 km. The consolidation was arrested at the Fairview water intake. The event caused some minor flooding of a greenhouse at Dunvegan Gardens and the 11 gauges downstream recorded the resulting surge. The ice front reached its furthest upstream position on February 5, 2004. Until late-March the ice front receded slowly and from then onwards it rapidly retreated downstream.

From November to January monthly mean temperatures in the test area ranged from below to above average. In response, the ice front progression fluctuated around the average. February to April temperatures were above average and caused the ice front to recede faster than average.

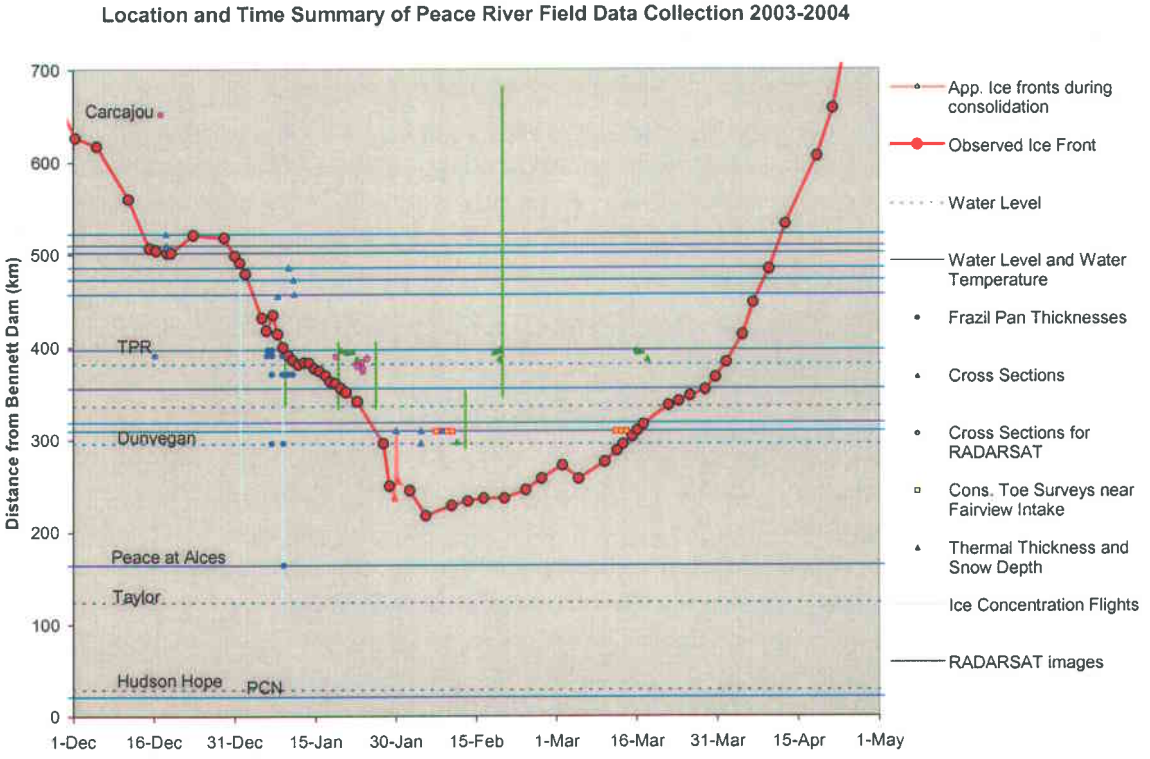

Figure 2 : Ice front progression and summary of the Peace River Data Collection 2003-2004

3 Data analysis and results

3.1 GIS implementation

The processing, analysis and interpretation of the images require several topographic data layers. They were integrated within the ArcGIS® software (ESRI).

For the land area adjacent to the river channel, we acquired digital elevation data at the 1:20 000 scale from ALTALIS (27 map sheets). For the remaining land area, the 'Canada 3D' elevation data were obtained at 1: 250 000 scale at no cost from the Center for Topographic Information (CTI) (http://www.cits.rncan.gc.ca/). By combining these two data sets, we then created a Digital Elevation Model (DEM) for the entire area of interest. The DEM data were used for orthorectification of the images and to calculate channel slope. Layers of roads, railways and the hydrography were acquired by BC Hydro from CTI's National Topographic Database at a scale of 1:50 000. In rural areas such as Northern Alberta, NTDB aims at attaining a circular map accuracy standard of 25m. However, the hydrographic layer provided was not accurate enough or/and out of date for the project's requirements (NTS sheets of the area of interest became valid in 1989 and are based on even older aerial photography). Instead channels, islands and sandbars were manually digitized from two recent Landsat-7 ETM images downloaded from Natural Resources Canada's Geogratis website (http://geogratis.cgdi.gc.ca/) (Table 2). These vectors were subsequently used to create a mask of the channel excluding all islands. Pass points on the Landsat-7 images were used to georeference the SAR images.

Table 2: Coverage of Landsat-7 images (Panchromatic band, 15m resolution)

Date of Landsat-7 image	Coverage
22 August 1999	From Dunvegan to Peace River
01 October 2002	From Peace River to Carcajou

The channel mask was used for the extraction of ice thickness information from the SAR data. Since ice jam thickness is a function of river width, the channel was subdivided into longitudinal 500m and 100m reaches. Figure 3a shows the 500m reaches. As described in Jasek at al. (2003), the polygons were created semi-automatically around evenly spaced centroids using a FORTRAN script.

The averaging polygons could alternatively be derived from physiographic parameters like channel width, depth, slope and sinuosity. It is speculated that physiographically homogeneous reaches may contain fewer ice cover types and, therefore, may render more representative ice thickness values than mathematically chosen polygons. With this method in mind, we have completed the channel width layer (Figure 3b) and the slope layer.

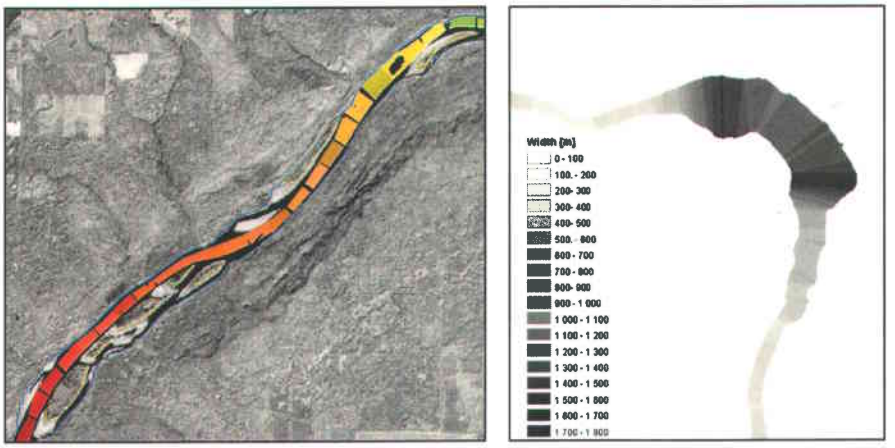

a) b)

Figure 3: a) Subset of the river 500m sections; b) Subset of the channel width layer

3.2 Image processing

For all RADARSAT and ASAR images, gray levels were radiometrically transformed into backscattering coefficients (power values) using a look-up table. This step was performed with the Geomatica™ software (PCIGeomatics). Subsequently, all images were georeferenced using GCPs from road vectors, corner reflectors and features from the already orthorectified Landsat images. Then the images were orthorectified using the DEM.

In preparation of the surface cover classification, two processes were tested (Table 3). The filtering method scales the entire images from 16 bits to 8 bits to reduce the computing time. Speckle is removed with the Kuan Filter and the image is smoothed with the Median Filter. The second method creates a texture image (8 bits) from the original 16 bit image, based on second-order statistics computed from the grey level co-occurrence matrices (P). In this case, the mean parameter is used (Mean_i = SUM(i,j=0,N-1)(i*P(i,j)).

Ice types are classified using the Fuzzy K-Mean unsupervised algorithm. This clustering algorithm segments the pixels under the river mask according to an iterative measurement of the distance to the class mean. For each pixel in the image, that pixel is assigned to a class such that the distance from this pixel to the center of that class is minimized. 'Fuzzy' means, that each pixel has a degree of membership in each cluster.

Table 3: Processing steps

Filtering method (Weber et al, 2003)	Texture method (Gauthier et al, 2003)
Backscatter (Powers,16 bits)	Backscatter (Powers, 16 bits)
Scaling (8 bits)	Texture (Mean parameter) 7X7 , 8 bits
Kuan Filter (5X5)	
Median Filter (5X5)	

For the ice thickness related part of the project, backscattering coefficients averaged over 500m and 100m sections along the channel were extracted.

3.3 Backscatter analysis

3.3.1 Longitudinal backscatter analysis

Backscattering profiles were extracted from RADARSAT and ASAR images. Figure 4 shows the averaged backscattering profile for 500m sections along the main channel for the four RADARSAT-1 images.

On January 10, an aerial survey located the ice front at kilometer 394. Upstream of the ice front, low to high concentrations of frazil pans, and open water were observed. On the backscatter profile the increasing concentration of frazil pans towards the head of the complete ice cover causes the rapid increase of the backscatter. Using the information from the aerial ice survey, the ice front ice front should, therefore, be located at the first peak above the -6dB threshold. However, this backscatter peak at kilometer 394 is rather small. A second, more pronounced peak is located at kilometer 395. This is probably where the head of the complete ice cover was located at the time of image acquisition. Downstream of the head of the complete ice cover, the ice cover ranged from juxtaposed to consolidated, with backscatter values varying between -7dB and -2dB.

According to the aerial survey, the ice front had progressed upstream to kilometer 356 on January 20. The head of the complete ice cover can clearly be detected at kilometer 356 on the backscattering profile. Again, it is located at the first peak above the -6dB threshold. For both dates, the shift from an incomplete to a complete ice cover is about 4dB.

On January 27 and February 20, the imaged channel is completely ice covered. After consolidation, the backscattering profile remains relatively stable over time, with a mean difference of 5% (0.17 dB). The texture also remains unchanged with only 1.3% variation.

The difference in the backscatter signal for consolidated ice between January 10 and February 20 is rather small and believed to be related to the incidence angle of the images. For example, between kilometer 396 and 406, the lowest backscatter corresponds to the F4 image, which has the largest incidence angle of the four images. Low signal return from an F4 image is to be expected because the backscatter is lower in the far range than in the near range. In contrast, the highest backscatter values are those of the F1N image, which has the lowest incidence angle. The two F2F images are in-between.

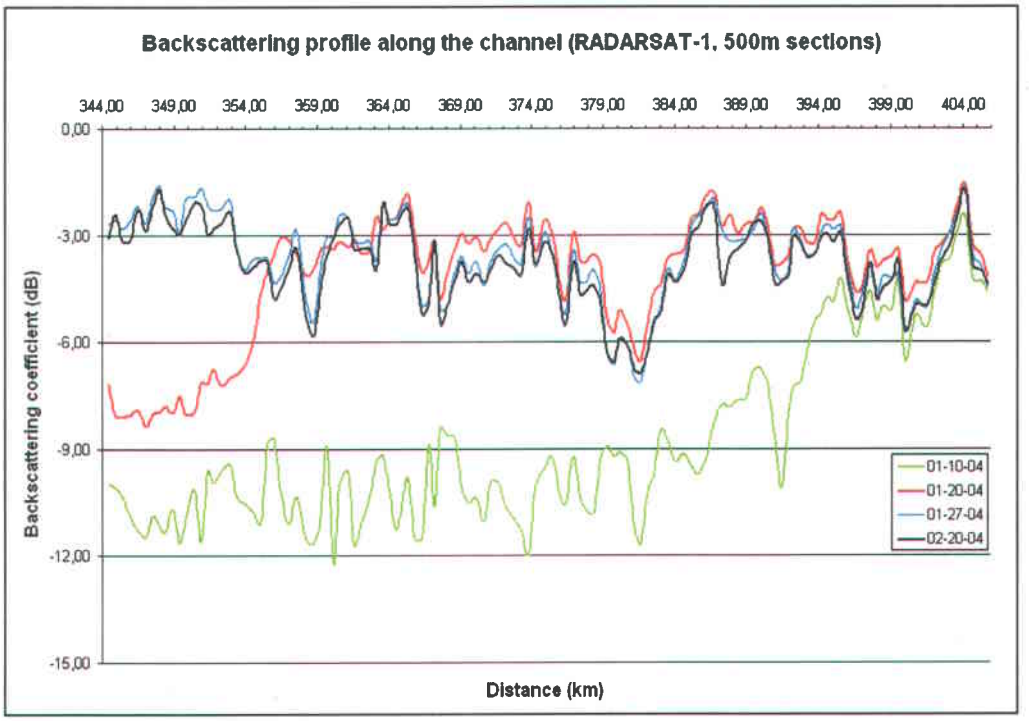

Figure 4: Backscattering profile of RADARSAT images (500m sections)

3.3.2 ENVISAT – RADARSAT-1 backscatter comparison

ENVISAT ASAR images were compared with RADARSAT-1 images in order to determine whether using ASAR data could increase SAR data availability.

Figure 5a shows, that despite differences in technology and spatial resolution, the pattern of backscatter profiles of ASAR-HH and RADARSAT-1 images is similar. However, the magnitude of ASAR-HH backscatter is slightly lower than that of RADARSAT-1. The reach imaged consists of a consolidated ice cover. The mean difference is 15% (-0.49dB) for the February 20 pair and 11% (-0.33 dB) for the Jan.27/Feb.1 pair. The texture difference is 12% in both cases.

As shown in Figure 5b for the February 1 image, there is no significant difference between backscattering profiles from ASAR HH and VV polarizations at the image resolution used. Similarly, backscatter of HH and VV polarized data from the February 20 image (not shown) are of the same magnitude. For these two images, the mean difference between HH and VV are 3.5% and 2.4%, respectively, with an R^2 above 0.90.

On the February 10 image, we observe a more significant backscattering variation (8.3%) and a much lower R^2, particularly with texture data (Figure 6). This is probably caused by warmer temperatures. On February 1 temperatures in the town of Peace River were between –21.7°C and –32.5°C. Temperatures before image acquisition on February 20 ranged from –18.5 to –1.8°C. In contrast, the temperature at image acquisition on February 10 was –4.6°C with the preceding 3 days all recording above freezing maximum temperatures (2.2°C, 4.2°C, 8.5°C). Therefore, the uppermost layer of the snowpack overlying the river ice may have contained some liquid water and, thereby, altered the signal response.

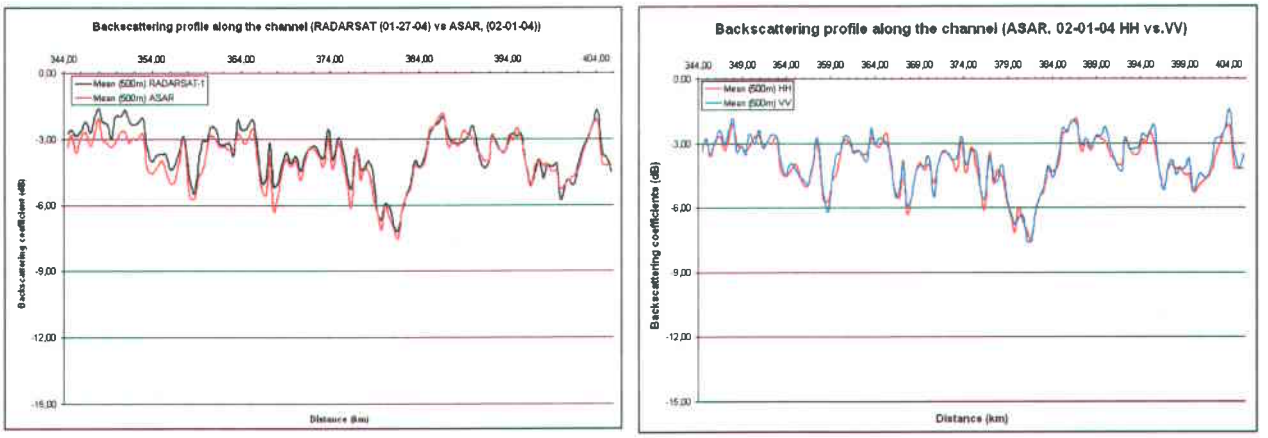

Figure 5: Comparison of backscattering profiles from a) RADARSAT vs ASAR-HH and b) ASAR-HH vs ASAR-VV images (500m sections)

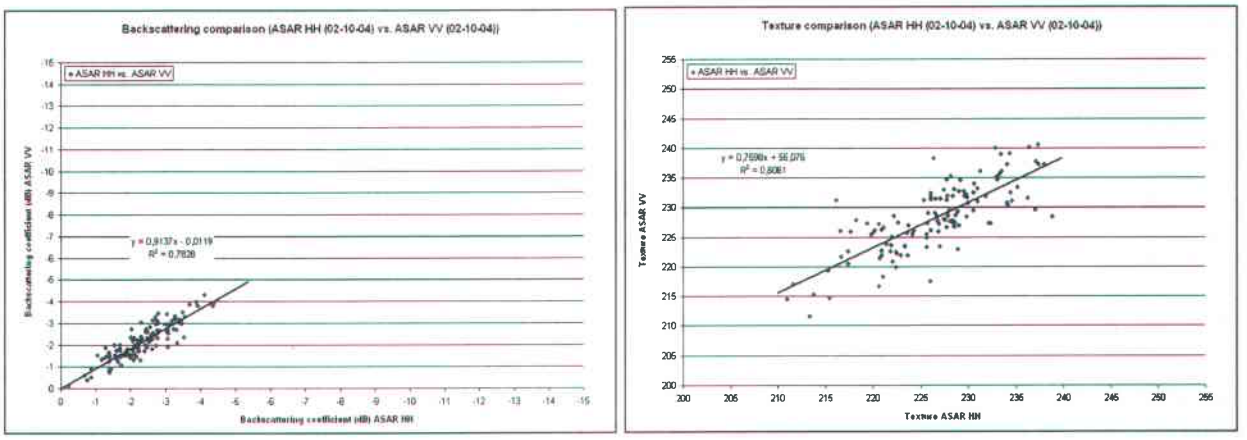

Figure 6 : Regression of a) backscattering data and b) texture data from the ASAR HH and VV images of February 10 (500m sections).

3.3.3 Backscatter derived ice thickness

An ice jam is the result of shoving. Figure 7 shows the typical components of an ice jam, which are the toe, the equilibrium section, and the head. The equilibrium section is characterized by a constant ice thickness, uniform flow, and the maximum water depth caused by the ice jam (Gerard et al. 1992). The ice jam is in equilibrium when the forces from the downslope component of the weight of the ice cover and the drag from the flow moving underneath are resisted by the accumulation's internal strength and bank shear. The ice accumulation's ability to transfer these downstream forces to the banks depends on its internal strength and thickness. The equilibrium ice jam equations determine the minimum ice thickness at which this force balance can occur (US Army Corps of Engineers 2002). High flows, steep channels, and wide channels produce thick ice jams. Due to flow regulation, the winter flows on the Peace River are high compared to unregulated rivers and river ice is consequently relatively thick. Ice thickness is thereby defined as the total ice thickness, which includes thermal ice, consolidated ice pans, and frazil slush.

It follows that the ice thickness and roughness are consistent with the equilibrium ice jam theory only between the shear lines. Therefore, only data between the shear lines was used to average the backscatter signal. Open water leads were removed on the basis of the classification results that will be discussed in the next section.

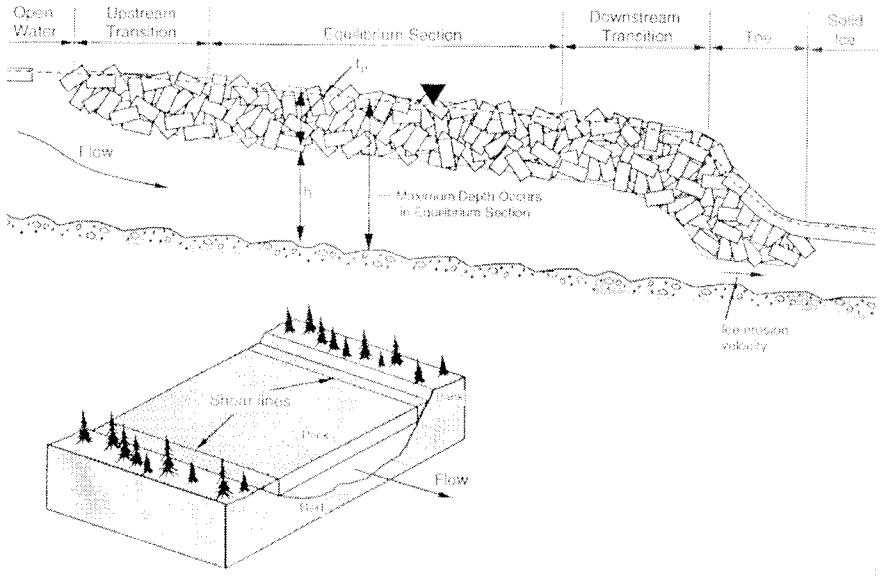

Figure 7 : Longitudinal profile through an ice jam (Gerard at al. 2004 : 23)

A quantitative relationship was established between RADARSAT backscattering coefficients and ice thickness measurements acquired on four cross-sections in the test area. Based on a very limited amount of data collected, the following results were obtained:

- In January, total ice thickness correlates significantly better with backscattering coefficients, than thermal ice only;
- In February, thermal ice thickness shows a slightly higher R^2 than total ice thickness (500m sections: 0.94 vs. 0.70, 100m sections: 0.87 vs. 0.80);
- In most cases, 500m reaches correlate better with backscatter than 100m reaches.

Jasek et al. (2003) correlated RADARSAT-1 backscatter with total ice thickness and sail height. The following results were obtained:

- A comparison of backscatter correlations with total ice thickness and sail height was inconclusive. Total ice thickness and sail height both correlated well with backscatter.
- Image and field data taken closest to ice cover formation correlated best and found an R^2 of 0.89 based on 7 data points.

This study concluded the following:

- The combined data from the 2003 and 2004 monitoring seasons (17 data points) resulted in an R^2 of 0.87 (Figure 8). Please note, that 500m averaged data were used in 2003, while 100m averaged data were used in 2004.
- The regression equation to derive total ice thickness backscatter is as follows: total ice thickness = 8.0996 * backscatter (power) – 1.1288.

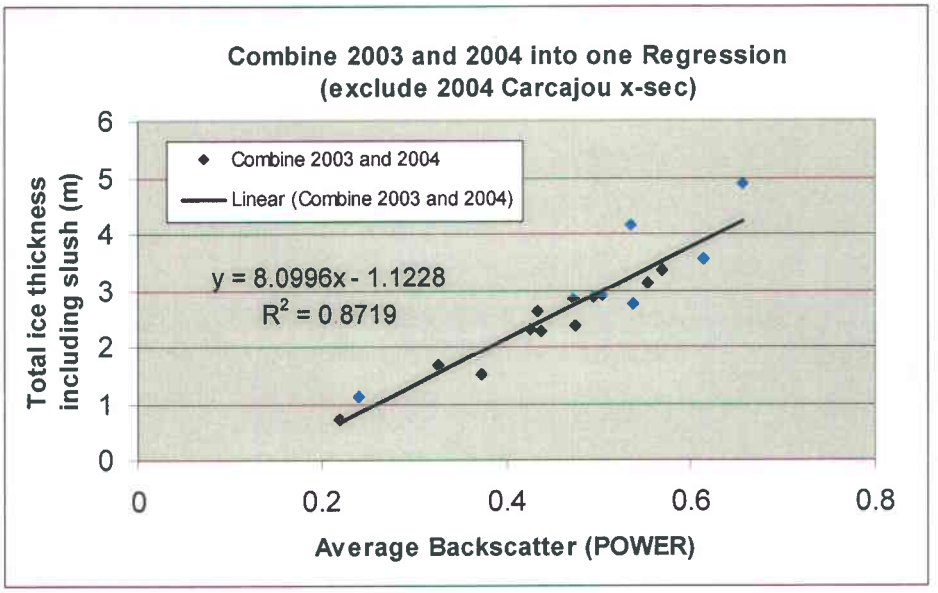

Figure 8: Regression between RADARSAT backscattering coefficients and ice thickness combined for the 2003 and 2004 monitoring seasons

Using the relationship between backscatter and total ice thickness established above, the total ice thickness on the Peace River for a 46km reach is calculated. In Figure 9 calculated and measured ice thickness for the 2004 winter are shown. The simulated ice thickness matches the measured one very well. Reaches of a thick and thin ice cover can be readily identified. Negative simulated ice thickness data, probably caused by open water, were manually removed.

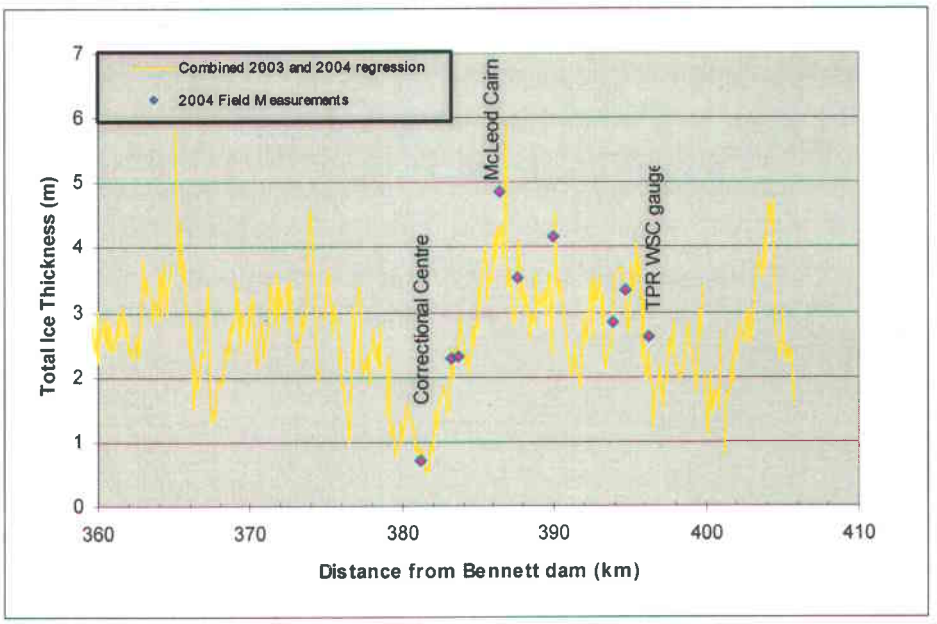

Figure 9: Calculated and measured total ice thickness on the Peace River during the 2004 winter

Figure 10 shows the calculated thickness using the combined 2003 and 2004 regression for 2003 and 2004 images at a 500 m resolution. Preliminary comparisons with water level profile data and jamming locations for the two years agrees well. For example, a consolidation occurred through the Correctional Centre reach in 2003 but not in 2004.

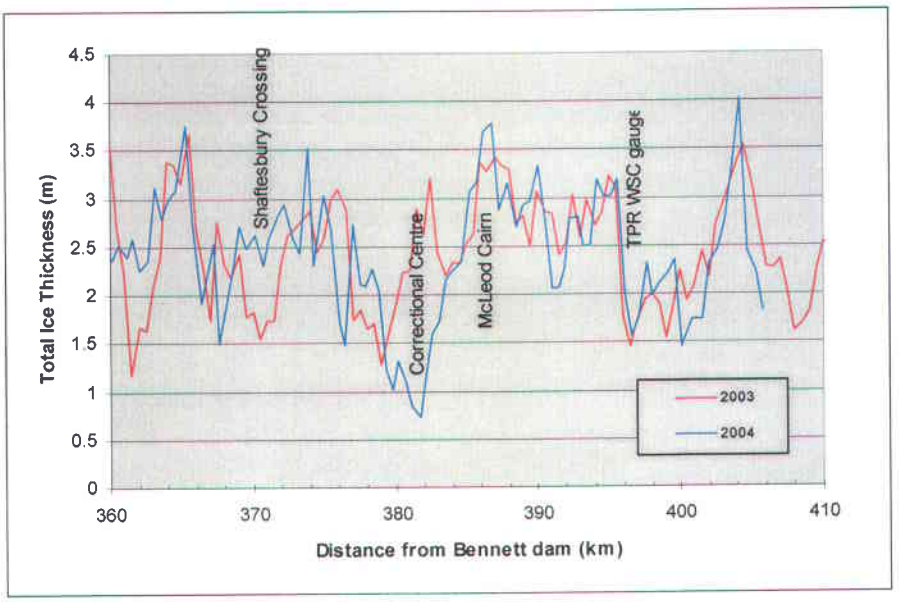

Figure 10 : Calculated total ice thickness on the Peace River for 2003 and 2004 from 500m polygon averages of RADARSAT backscatter power.

3.4 Classification of SAR images and ice cover type mapping

The objective of this classification is to accurately map the spatial distribution of ice cover types on the river. The number of classes should match the number of surface cover types on the river. This is not an easy task as the definition of what exactly constitutes a particular ice cover type is at this stage somewhat arbitrary. The boundaries between individual ice cover types are not always clearly visible by the naked eye. Therefore, validating the ice cover classification of the satellite imagery proves difficult and remains subjective.

The number of classes was initially set to seven, which corresponds to the range from smooth water with minimal backscatter to heavily consolidated ice with maximum backscatter. Following are surface cover types to be expected on the Peace River during the freeze-up period:

- Open water
- Frazil pans (low and high concentrations)
- Freeze over border ice
- Juxtaposed ice
- Consolidated ice (light and heavy degree of consolidation)

A comparison of the classification results from the filtering and texture method suggests that the texture method is better at discriminating low backscattering targets such as open water, frazil pans, freeze-over border ice. In contrast, the filtering method more accurately discriminates high

backscattering targets, such as consolidated ice (Figure 11 and Figure 12). The difference in sensitivity between both methods is due to the asymmetrical distribution of data fed into the classification (Figure 13). The histogram of the backscattering power values is skewed toward the low values, resulting in more discrimination within the higher classes. The histogram of texture is skewed toward the high values, resulting in more discrimination within the lower classes.

We have, therefore, tested several ways of combining the two methods. The best results were obtained by a two step approach:

1. Seven classes are outlined with the texture method
2. A mask is put over the highest class and the filtering method is used to create two new classes instead. This provides a modified class #7 and a new class #8 (Figure 14).

The combined classification method was applied to six RADARSAT-1 images which were acquired on February 13 and 20, 2004 and covered the extended research area. Due to file size and processing time, each image was classified separately and the resulting maps were subsequently combined into two maps. One map covers the section upstream of TPR (Figure 15) and the other one covers the section downstream from TPR (Figure 16). For the most northerly image near Carcajou, pass points were scarce and no accurate georeferencing was possible. The image was, therefore, not processed. Also, it was concluded that, due to overlapping, three images would suffice in the future to cover the river reach downstream of TPR.

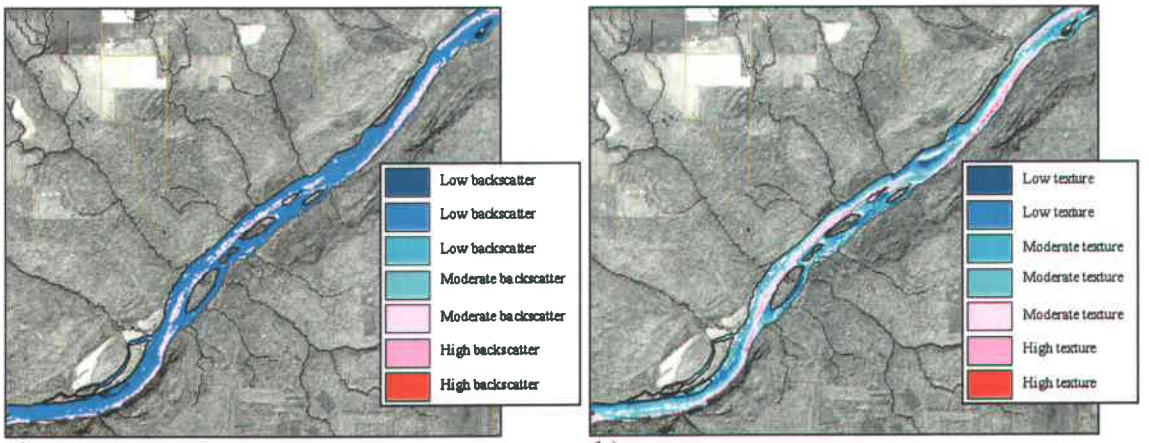

Figure 11: Classification results using the filtering (a) and texture (b) methods for a reach upstream of the ice front (km340-357). RADARSAT-1 image - January 10, 2004. The river flows from the bottom left to the top right.

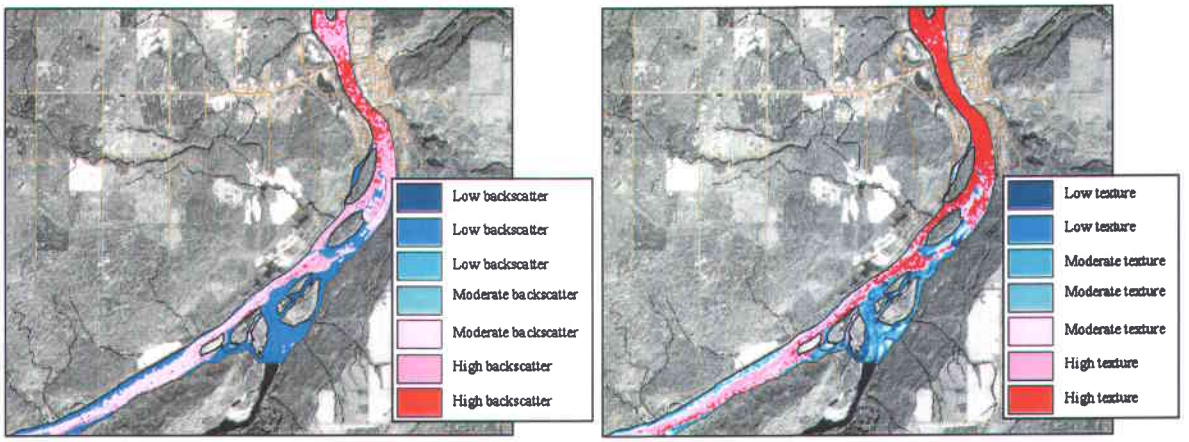

a) b)

Figure 12: Classification results using the filtering (a) and texture (b) methods for a reach near the ice front (km382-398). RADARSAT-1 image - January 10, 2004. The river flows from the bottom left to the top centre

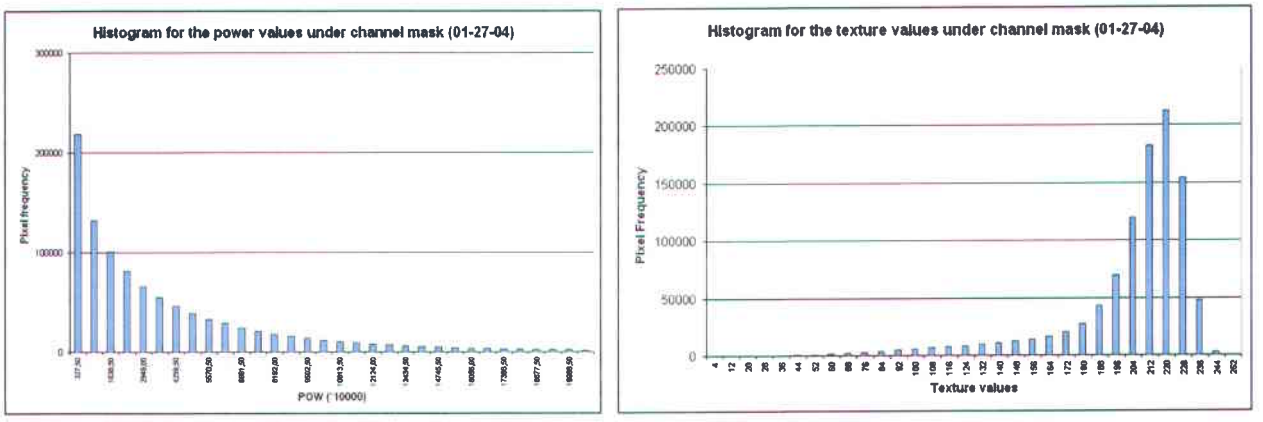

Figure 13: Histograms of power and texture images for January 27, 2004.

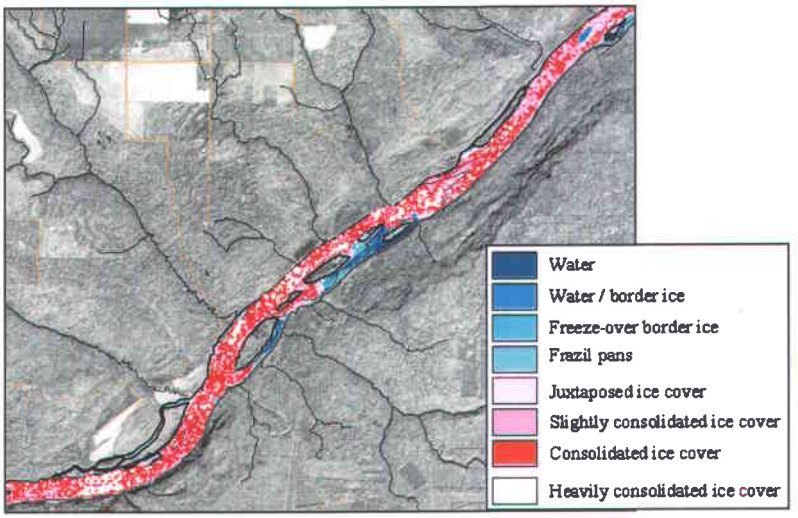

Figure 14: Results from the combined classification for a river reach with consolidated ice (km340-357) – RADARSAT image - February 20, 2004. The river flows from the bottom left to the top right.

The combined classification was also applied to the ASAR images (not shown). Due to the relatively coarse resolution of 30m, ASAR is more likely to contain single pixels that contain several ice cover types. Therefore, the SAR signal response from an individual pixel will be an average of several ice types. Small features, such as small open water leads, were occasionally missed. When using both vertically and horizontally polarized ASAR images as input to the classification process, the results deteriorated. This is probably due to speckle caused by the high correlation between the two channels. In general, horizontally polarized ASAR images (HH) produced results similar to that of RADARSAT-1 images, which are also horizontally polarized (HH). It was concluded that ASAR images could provide a viable and cheap alternative to RADARSAT-1 images. However, the reliability ASAR in operational mode should be assessed.

The ice cover classes as determined by the classification of the February 13 and 20, 2004 images were verified through visual comparison of selected sites with photographs taken during the aerial survey on February 20, 2004. For example, Figure 17 shows the large ice toe near the Fairview water intake (km 309), which formed on January 30 after a consolidation event. The ice ran for 76km and produced walls 6m high above the water level. The total ice thickness reached 11m. The insert in Figure 17 displays the full ice classification, while class #8 was superimposed onto the georeferenced aerial photo. Areas of heavy consolidation match class #8 very well. Some areas were mis-classified into class #7. This is probably due to incorrect histogram segmentation by the classifier, inaccuracies in the georeferencing process, and pixel resolution.

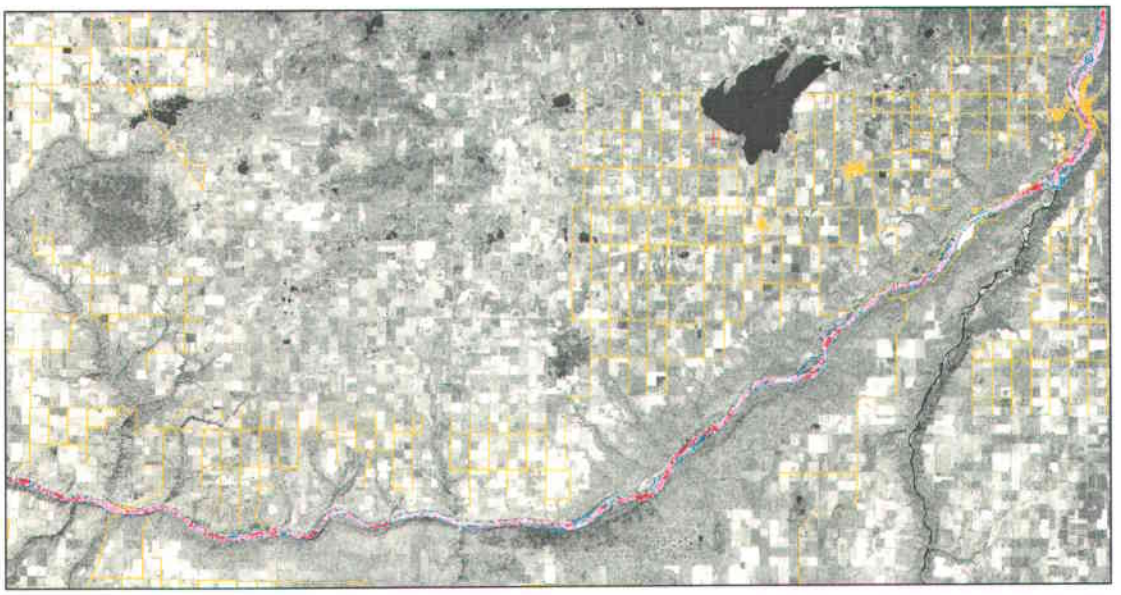

Figure 15: Mosaic of the two classifications upstream from TPR

Figure 16: Mosaic of the four classifications downstream from TPR

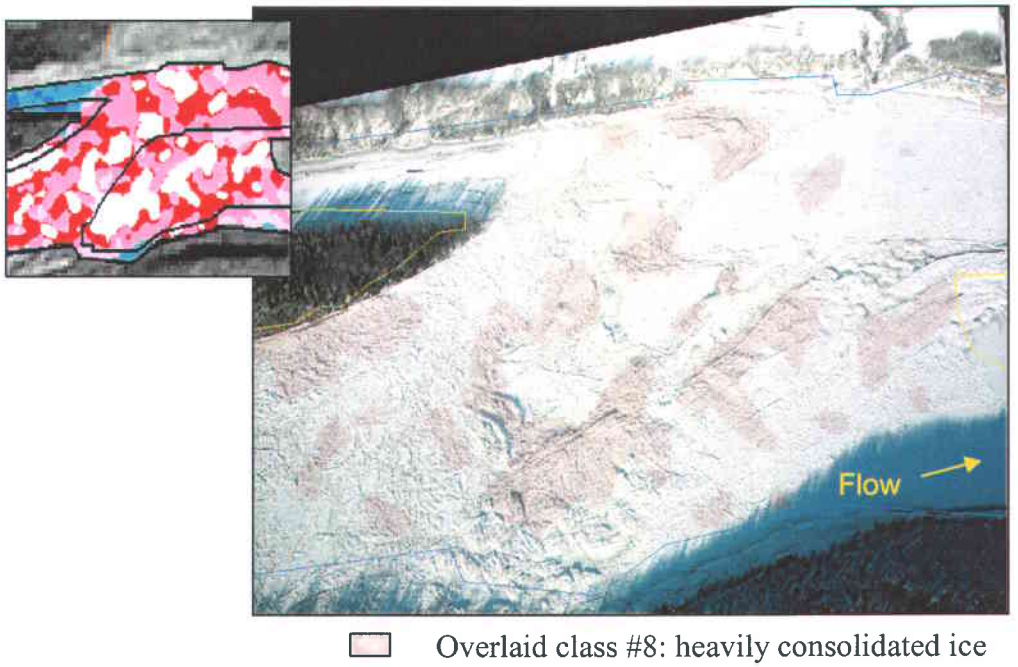

Figure 17: Photo of an area of heavy ice consolidation, with a transparent overlay of class #8 (heavily consolidated ice) from the combined classification.

3.5 Incidence angle analysis

To assess the sensitivity of river ice backscattering to the incidence angle, we have used two image pairs that were available from the 2000-2003 Peace River experiment (Table 4). These two image pairs were selected, because the ice properties are believed to not have changed significantly between the acquisition dates of an image pair. Also, the images of a pair had to have a different look direction or incidence angle. Images were radiometrically transformed and georeferenced. An incidence angle image was created for each image.

Table 4 : Image pairs used for incidence angle analysis

Pair	Acquisition date	Beam	Orbit
Pair 1	24 January 2002	F2	Ascending
	30 January 2002	F1	Descending
Pair 2	25 February 2003	F1	Descending
	04 March 2003	F4	Descending

Test sites were selected in homogeneous areas of the ice cover and backscattering coefficients were extracted along with the corresponding incidence angle. The incidence angle variation over a single RADARSAT-1 Fine Beam Mode image is small (3 degrees). However, the incidence angle difference between Fine Beam Mode 1 and Fine Beam Mode 5 can reach 13 degrees. Within one image, incidence angles at the selected test sites differed by a maximum of 2 degrees. Between two images, the same site could be seen with a maximum difference of 4.5 degrees, resulting in a maximum backscattering difference of 1dB. Considering the small incidence angle differences between available datasets from test sites, we chose not to continue analyzing the datasets from test sites, but instead explore a theoretical mathematical approach.

Backscattering coefficients acquired under a specific set of incidence angles were transposed to values corresponding to a different set of incidence angles. In this way, data from F1 and F4 beams could be compared. The method consists of the following steps:

1. Refraction angles are calculated at each test site

2. Refraction angles are plotted against backscattering coefficients for all tests sites for a single image

3. Regression slopes for all data pairs of a single image with at least a 0.5 degree difference are calculated

4. Considering that we have a linear relationship of the form "Backscattering Coefficient = a * Refraction Angle + b", we can use the known backscattering coefficients of the test sites to estimate parameter b for all previously calculated slopes. Then, we alternately apply all these different linear relationships to the test sites.

5. As we know from initial observations, there should be a maximal variation of 1dB between the two images of a pair. We therefore eliminate all slopes that resulted in larger variations.

6. From the remaining slopes, we calculate the mode. This most often occurring slope is selected for the final algorithm.

7. The final algorithm is applied to the second image of a pair. The calculated backscatter is compared to the observed backscatter.

This algorithm is based on the first image of a pair and provides backscattering coefficients corresponding to the incidence angles of the second image. It has been tested on the two available pairs, in both directions. Results are presented in Table 5. Before standardization, the mean backscattering difference between test sites was in the order of some tenths of dBs. The standardization process reduced the difference to one hundredth of dBs.

Although this approach is based on few datasets and therefore has only been tested with a small range of backscattering coefficients and incidence angles, the results are promising and will be further investigated.

Table 5 : Results of the standardization

Image pair	Backscattering difference		Backscattering difference		
	Before standardization		After standardization		
	Mean	STD	Mean	STD	
January 24 vs January 30, 2002 (F1,F2)	- 0,31	± 0,28	-0,04	± 0,25	From Jan 24 to Jan 30
			-0,03	± 0,25	From Jan 30 to Jan 24
February 25 vs March 4, 2003 (F1,F4)	-0,68	± 0,14	-0,05	± 0,14	From Feb 25 to Mar 4
			-0,09	± 0,14	From Mar 4 to Feb 25

3.6 Operational application

The ice cover type classification of river ice affected rivers, which was developed as part of this project, was operationally applied on the Des Prairies River (Quebec) on January 17, 2005. A RADARSAT-1 image was acquired in emergency mode by CSA, pre-processed and delivered within hours by RSI. The images were manually orthorectified by INRS. Ice maps were automatically produced and transferred to the interested authorities, in this case the Government of Quebec, through a Geoconference® session (TGIS Consultants) in less than 24 hours after image acquisition (Figure 18). Based on the ice cover type maps produced, the Government of Quebec identified 'hot spots' on the river to which they sent field crews.

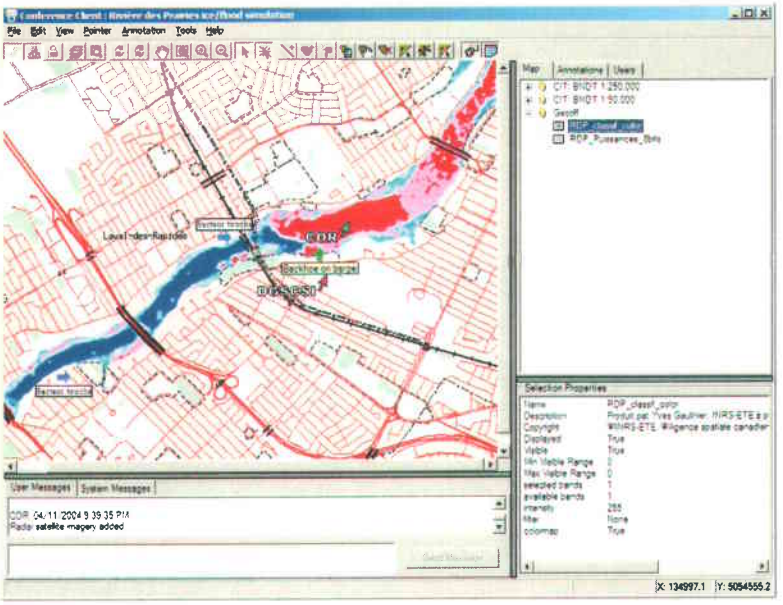

Figure 18 : Example of a Geoconference session, where the ice map is shared and discussed through a georeferenced teleconference on Internet.

4 Conclusions

The operation of BC Hydro's hydropower generation facilities on the Peace River, British Columbia and Alberta, requires detailed knowledge of river ice processes. This project under the Strategic Investment Initiative successfully continued the river ice work done previously by BC Hydro and significantly improved remotely sensed river ice products through the expertise of the scientific community:

1. The data collected in this project confirmed a significant relationship between backscattering coefficients and observed ice thickness. In this study the backscatter from images obtained under various incidence angles were used. The relationship between backscattering coefficients and observed ice thickness could be further improved once the algorithm to standardise backscattering coefficients from images acquired at different incidence angles is operational (see 5.). Also, the correlation should be redone using 100m averaged backscatter for all years used.

   The relationship developed could potentially be used to derive total ice thickness from radiometrically corrected RADARSAT-1 images, which in turn could be used to verify hydraulic river ice models. The data could also be used to establish a database of typical ice thickness along the river. In a given year, ice thickness could operationally be compared to historical ice thickness and abnormalities could be detected.

2. A new approach to image processing involved texture analysis of SAR images. It was demonstrated that a combination of texture analysis and traditional filtering methods improves the delineation of low backscattering ice cover types without compromising the delineation of high backscattering ice cover types.

3. Ice cover type maps were created which clearly showed the location of the head of the complete ice cover and the spatial distribution of ice cover types upstream and downstream of the head of the complete ice cover. The head of the complete ice cover could also be located on backscatter profiles of the river. The ice cover maps could be used operationally to determine, for example, the head of the complete ice cover, the intensity of frazil ice production, and monitor consolidation events.

4. The results of this study suggest that SAR availability can be increased using both RADARSAT-1 and ASAR imagery. ASAR images represented a complementary source of data for river ice monitoring. The reliability ASAR in operational mode should be assessed

5. We have also proposed an algorithm to standardise backscattering coefficients from images acquired at different incidence angles. However, the procedure is not operational yet.

6. Finally, we have developed and demonstrated the feasibility of a process to semi-automatically analyse SAR data and disseminate ice cover type maps in near real-time to end-users.

This project built on several previous river ice studies by the partners involved as well as other agencies. At this point, the development of the data products is in an advanced stage. The classification of ice cover types is possible with a relatively high degree of confidence. In particular, the dominant ice cover types and thus ice cover producing processes can be clearly gleaned from the maps. The ice cover maps are highly self-explanatory and require minimal river ice specific knowledge for interpretation. However, misclassification of ice cover types still occurs and could be reduced, for example, by making use of topographic information.

Also, significant improvements in the understanding of radar - river ice interactions could be made by physically modeling the radar return from river ice. Image coverage of the area of interest on the Peace River is high, in particular when using both RADARSAT-1 and ASAR images, and is expected to suffice for operational use. It is recommended to conduct a cost-benefit analysis of producing remotely sensed river ice data products.

5 References

- Gauthier, Y., El Battay, A., Bernier, M., Ouarda, T., 2003. An approach using contextual analysis to monitor river ice from RADARSAT data. Proceedings of the 60th Eastern Snow Conference, June 2003, Sherbrooke, Canada.

- Gerard R., M. Jasek, and F. Hicks. 1992. Ice Jam Flood Assessment – Yukon River at Dawson. Unpublished report prepared for Indian and Northern Affairs Canada, Whitehorse, Yukon.

- Jasek, M., Weber, F. and Hurley, J. 2003: Ice thickness and roughness analysis on the Peace River using RADARSAT-1 SAR imagery. Proceedings 12th Workshop on the Hydraulics of Ice Covered Rivers, Edmonton, AB, June 19-20, 2003.

- United States Army Corps of Engineers. 2002. Hydraulic Computaton and Modeling of Ice-Covered Rivers. http://www.usace.army.mil/inet/usace-docs/eng-manuals/em1110-2-1612/c-4.pdf. Accessed June 2005

- Weber, F., Nixon, D. and Hurley, J. 2003. Semi-automated classification of river ice types on the Peace River using RADRASAT-1 Synthetic Aperture Radar (SAR) imagery. Can.J.Civ.Eng. Vol. 30, 2003: 11-27.